Hindawi
Geofluids
Volume 2022, Article ID 2472280, 13 pages
https://doi.org/10.1155/2022/2472280

Research Article

Experimental and Numerical Analysis of Flow Behavior for Reverse Circulation Drill Bit with Inserted Swirl Vanes

Cheng Yang,[1] **Jianliang Jiang**,[1] **Bo Qi**,[2] **Guoqing Cui**,[2] **Liyong Zhang**,[1] **Yunwang Chen**,[2] **and Pinlu Cao**[2]

[1]*Zhejiang Engineering Survey and Design Institute Group Co. Ltd., No. 501 Liyuan South Road, Ningbo City 315012, China*
[2]*College of Construction Engineering, Jilin University, No. 938 Ximinzhu Str., Changchun City 130061, China*

Correspondence should be addressed to Pinlu Cao; jlucpl@jlu.edu.cn

Received 16 September 2021; Accepted 1 December 2021; Published 8 January 2022

Academic Editor: Shengnan Nancy Chen

A swirling drill bit designed with an integrated vane swirler was developed to improve reverse circulation in down-the-hole hammer drilling. Its entrainment effect and influential factors were investigated by CFD simulation and experimental tests. The numerical results exhibit reasonable agreement with the experimental data, with a maximum error of 13.68%. In addition, the structural parameters of the swirler were shown to have an important effect on the reverse circulation performance of the drill bit, including the helical angle and number of spiral blades, swirler outlet area, and the flushing nozzles. The optimal parameters for the swirling drill bit without flushing nozzles include a helical angle of 60°, four spiral blades, and the area ratio of 2, while it is about 30°, 3, and 3 for the drill bit with flushing nozzles. Moreover, the entrainment ratio of the drill bit without flushing nozzles can be improved by nearly two times compared with one with flushing nozzles under the same conditions.

1. Introduction

Swirling flows which always lead to strong shear and centrifugal forces have been utilized in many industrial applications. For instance, creation of swirling flows in high-intensity combustion systems would result in recirculation zones which further stabilize flames [1, 2]. Dong and Rinoshika [3] initiated swirls in the flows of carrier fluids to enhance fluid velocities and the associated migration of the particles carried by the fluids. Swirls introduced into a multiphase separator would contribute to strong centrifugal forces that can separate solid particles from solid-fluid mixtures [4]. Balakrishnan and Srinivasan [5] suggested that generating swirling flow is an effective way of reducing noise in subsonic free jets.

A swirling flow can be generated by many kinds of swirl generator [6], such as guiding vanes, tangential intake swirler, annular swirler, rotating mechanical devices, and honeycomb generator. Extensive experimental, analytical, and numerical studies that focus on swirling flows have been published in literature [7]. Yehia et al. [8] completed computational fluid dynamics (CFD) simulations of working fluid behaviors in the shell and tube heat exchangers with swirlers inside. Their simulations were utilized to investigate the effect of a swirler's geometry on heat transfer and friction loss in a shell and tube exchanger. Wen et al. [9] designed ellipsoid and helical blades aiming to generate strong swirls in the natural gas flows through supersonic separators. Wen et al. [9] further built an analytical Reynolds stress equation model as a quantitative evaluation of the supersonic separators' performance. In the same year, Funahashi et al. [10] used high-speed camera to observe two-phase swirling flows in a gas–liquid separator with three pick-off rings. Visualization experiments of gas-liquid two-phase swirl flows were also carried out by Liu and Bai [11] in a circular straight pipe.

Reverse circulation drilling with pneumatic down-the-hole (DTH) hammers is extensively utilized in mining, civil infrastructure, geothermal energy recovery, underground infrastructure, etc [12–14]. Figure 1 displays a schematic of

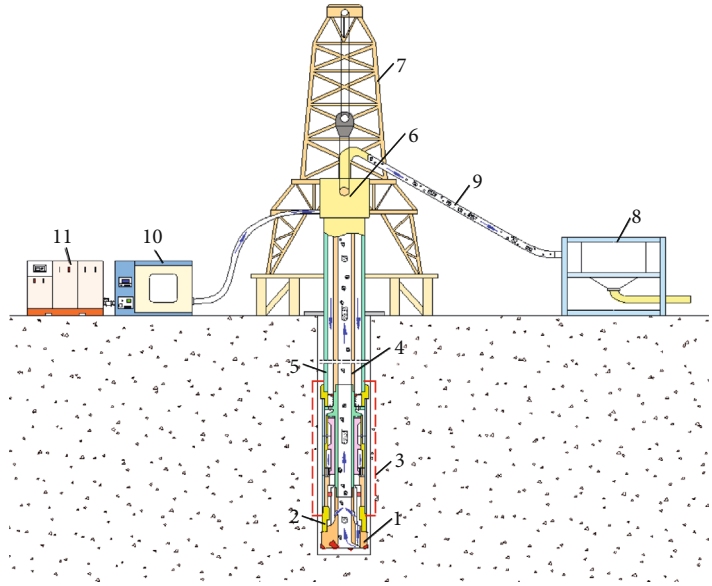

Figure 1: Reverse circulation drilling with DTH. 1: drill bit; 2: splined sleeve; 3: DTH; 4: inner drill pipe; 5: outer drill pipe; 6: swivel with double channels; 7: drill tower; 8: cyclone separator; 9: air hose; 10: air booster; 11: air compressor.

reverse circulation drillings through geological formations. During the drilling process, compressed air goes all the way down from land surface through the annulus between inner and outer drill pipes. Then, the air carries rock cuttings upwards from bottomhole through the central passage of inner drill pipe. Since the air is reversely circulated within drill pipes, air circulation loss into broken borehole or fractured formation can hardly happen. In addition, rock cuttings are safely isolated from borehole (see Figure 1), which benefits borehole stability through unconsolidated zones. Moreover, all the dusty air and rock cuttings carried to land surface are directly transported into cyclone separator [15]. Therefore, reverse circulation drilling is an environmentally friendly technology.

One of the most critical missions during a reverse circulation drilling process is to inhibit air leakage into borehole. Typically, two types of drill bits are designed for preventing the air leakage: one is the drill bit wrapped by a shroud, and the other is the drill bit with nozzles inside. Figure 2(a) shows the first type of the drill bits. A shroud is added around drill bit with an expectation of eliminating the clearance between drill bit and borehole [16, 17]. However, no perfect seal to the clearance can be guaranteed when borehole is broken into irregular shapes or the shroud wears out. Moreover, the shroud temporarily loses its sealing capacity when drilling through a big void space. Therefore, the upward transport of rock cuttings may be interrupted until the drill bit leaves the void zone, and the shroud regains its sealing capacity. Figure 2(b) displays the inside structure of the other type of drill bit. Flushing nozzles and suction nozzles are placed inside the drill bit body. As can be seen in Figure 2(b), high-speed air ejections out of the suction nozzles would create a low-pressure zone nearby. This low-pressure zone draws rock cuttings into the central passage of the drill bit. A number of experiments [13, 18, 19] in literature have explored the influence of a suction nozzle's structure, location, and inclination angle on the air circulation. Wu et al. [20] ever utilized CFD simulations to predict the performance of a drill bit when supersonic jets were added onto suction nozzles. Later, another layer of suction nozzles was added into the drill bit, hoping to improve the air circulation in drill bits. The improvement was not obvious though, since the streams of air ejected from different suction nozzles can interfere with one another, which results in a greater loss of energy. But this operation backfires. Air ejections from suction nozzles interfere with each other, which results in significant loss of energy in air circulation. In order to remove this adverse effect caused by suction nozzles, Cao et al. [21] designed an annular slit as a replacement of suction nozzles. Air ejected out of the annular slit would directly flow upward without creating flow interference. Despite all those efforts, the design of drill bits for reverse circulation drilling is far from perfect. An annular gap may occur between drill bit and borehole when the drill bit is drilling through fractured formations. Dusty air could possibly escape upward through the gap, causing environmental pollution and harm to drilling workers' health. In some cases, flushing nozzles must been removed for a more efficient air circulation at the cost of high drill bit temperature. It is concluded that more research is in demand to improve the reverse circulation within a drill bit.

Similar to the above exchangers and separators, swirls can also play their strength in reverse circulation drillings with pneumatic DTH hammers. Swirling flows bring about very strong suction forces toward rock cuttings. We ever designed a drill bit with a guide vane built in [6]. Our preliminary numerical simulations verified the role of swirling flows in improving the reverse circulation within drill bits [6]. This study is aimed at further investigating how the

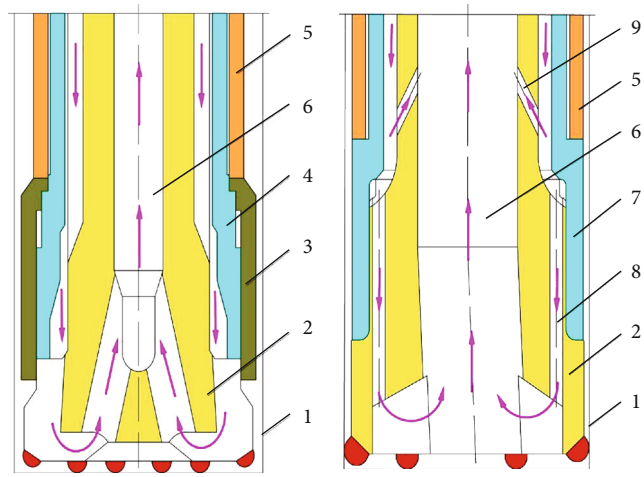

(a) Drill bit with a shroud (b) Drill bit based on ejector

FIGURE 2: Drill bit with reverse air circulation. 1: borehole wall; 2: drill bit body; 3: shroud; 4: drive sub; 5: hammer casing; 6: central passage; 7: connector; 8: flushing nozzles; 9: inner suction nozzles.

geometry of a guide vane swirler affect the reverse air circulation by virtue of both experiments and CFD simulations. Optimum design of vane swirlers can be chosen based on our experimental and numerical studies.

2. Reverse-Air-Circulation Drill Bit with Swirler

2.1. Working Principle of Reverse-Air-Circulation Drill Bit with Swirler. Figure 3(a) shows a schematic of vane swirler located fit inside a drill bit. Figure 3(b) gives an example of air circulation within the drill bit. The vane swirler's outer surface is designed to present evenly distributed spiral blades. Two flushing nozzles and six evenly distributed suction nozzles are found in upper drill bit body. The flushing nozzles stand vertically, while each of the suction nozzles are set at an angle of 45° with respect to the axial direction. Air flows down along an annulus between inner and outer drill pipes. A part of the air then rushes into suction nozzle. Next, this part of air gets ejected from the vane swirler at a high velocity, creating a low-pressure zone filled by swirling flows. The remaining air flows through flushing nozzles. Such air flow would cool down carbide inserts and sweep the rock cuttings away from bottomhole. Then, mixture of air and the rock cutting are drawn towards the low-pressure zone. This is entrainment resulting from swirling flows. The mixture would continue to flow upward into the cyclone at the surface. In cases of drilling through ultrabroken or cavity formations, the flushing nozzles can be sealed to let all compressed air ejected from the swirler, thereby enhancing its suction effect.

Three streams of air flow occur in the reverse air circulation within a drill bit—the primary one is air ejection from the vane swirler, the secondary one is the air flow through flushing nozzles, and the third stream refers to the air flow between the drill bit and the annulus among the drill bit and borehole. An entrainment ratio η_0 is defined as one of the indicators evaluating a drill bit's performance:

$$\eta_0 = \frac{m_3}{m_0} \times 100\% = \frac{m_3}{m_1 + m_2} \times 100\%, \tag{1}$$

where m_1, m_2, and m_3 represent mass rate of the primary, secondary, and third air stream, respectively. Mass flow rate m_0 equal to the summary of m_1 and m_2. Generally, a higher entrainment ratio corresponds to better air circulation. For a drill bit without flushing nozzles, the entrainment ratio is written as

$$\eta_0 = \frac{m_3}{m_0} \times 100\% = \frac{m_3}{m_1} \times 100\%. \tag{2}$$

A vane swirler's geometry is related to its resistance towards inflow air. Therefore, air mass flow rate m_1 varies with the vane swirler's structure. Therefore, air mass flow rate m_2 also changes at the given operating conditions, which will further greatly affect the efficiency of the swirler and the drill bit.

2.2. Design Parameters of Swirling Drill Bit. In this study, our drill bit is designed based on a classical reverse circulation air hammer DTH-89. Figure 4 shows views of our novel drill bit, and Table 1 lists key structural parameters of the drill bit. As can be seen in Figure 4, three parameters can fully describe the vane swirler in our drill bit—central angle θ, vane blade's helical angle α, and the total number of blades n. Total surface area A of n spiral slots is

$$A_s = \left(1 - \frac{n \cdot \theta}{360}\right) \times \frac{\pi}{4}\left(D_4{}^2 - D_5{}^2\right), \tag{3}$$

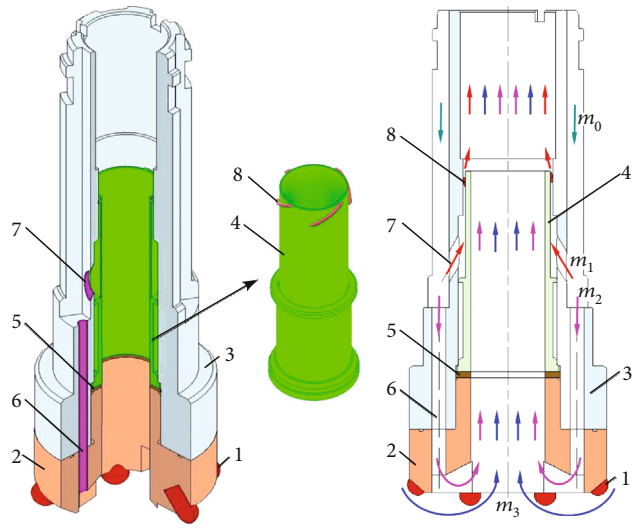

(a) Swirling drill bit structure (b) Working principle

Figure 3: Swirling drill bit. 1: carbide inserts; 2: lower drill bit body; 3: upper drill bit body; 4: swirler; 5: sealing; 6: flushing nozzles; 7: inner suction nozzles; 8: spiral blade.

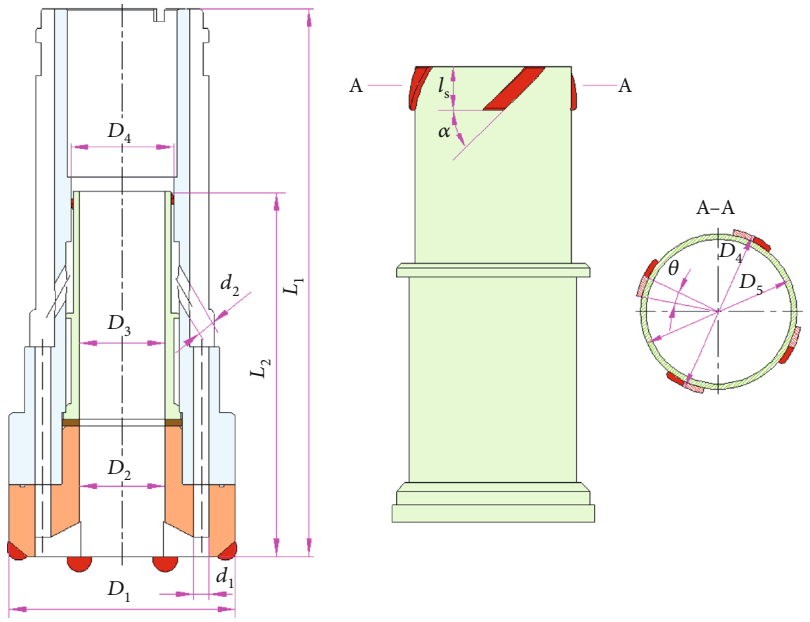

Figure 4: Views of the novel drill bit with a vane swirler inside.

Table 1: Structural parameters of drill bit with a vane swirler.

D_1, mm	D_2, mm	D_3, mm	D_4, mm	D_5, mm	L_1, mm	L_2, mm	d_1, mm	d_2, mm	l_s, mm
90	33	33	38	35.5	303	210	5	10	10

where D_4 and D_5 refer to outer and inner diameters of the vane swirler, respectively. Total cross-section area A_f of flushing nozzles is

$$A_f = \frac{3}{4}\pi {d_1}^2, \tag{4}$$

where d_1 is the diameter of a flushing nozzle's cross-section. Finally, ratio of spiral slot's outlet area over flushing nozzles' cross-section area, λ, becomes

$$\lambda = \frac{A_s}{A_f} = 2.45\left(1 - \frac{n \cdot \theta}{360}\right). \tag{5}$$

When studying the influence of swirler parameters on drill bit performance, and the effect of a single parameter is considered, values of other parameters are fixed at their original or optimal values.

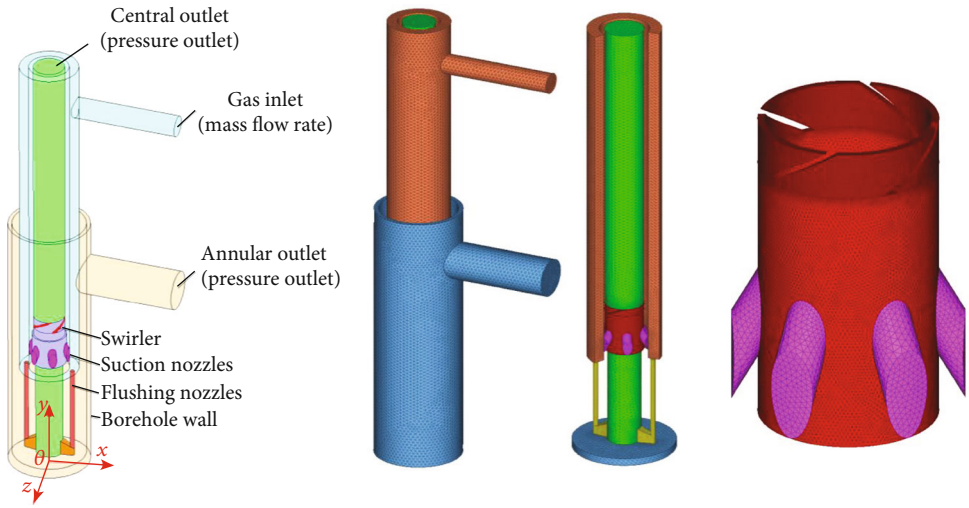

(a) Computation models (b) Computation grids

Figure 5: Geometry model and grid generation for the reverse circulation drill bit with a vane swirler built in: (a) computation models; (b) computation grids.

3. Numerical Solutions

3.1. Modeling and Mesh Generation. We build ANSYS fluent numerical models of the reverse air circulation within our novel drill bit. In our numerical models, borehole is assumed to be perfectly smooth. We consider that tungsten carbide inserts have negligible effect on the air circulation. Moreover, the influence of drill bit rotation on the air circulation within our drill bit is also neglected. A 10 mm clearance is set between bottomhole and the drill bit's bottom. Furthermore, the clearance between drill bit and borehole is set as 5 mm.

Figure 5(a) displays the 3D geometry model of our novel drill bit with a vane swirler built in. Then, this geometry model is taken into Hype-Mesh for gridding. Figure 5(b) provides a schematic of the meshes generated by Hype-Mesh. Both structured and unstructured body-adaptive meshes are generated in the domain of our drill bit. In addition, mesh refinement is applied in the vicinity of the vane swirler with an expectation of accurately simulating the air flows around. Accuracy of an air flow simulation on our drill bit strongly depends on mesh density (or number of meshes). Six numerical simulations of different mesh densities have been completed. Table 2 summarizes number of meshes in each of the numerical simulations and the corresponding simulation results including mass flow rates m_0 and m_3. Dependence of our numerical simulations' accuracy on mesh density is analyzed based on values of the mass flow rate m_3. As can be seen in Table 2, values of the mass flow rate m_3 becomes stable when the number of meshes varies in a range of (0.85 million, 1.23 million). Therefore, the final number of meshes in our drill bit model is chosen to be 0.85 million.

3.2. Boundary Conditions and Initial Conditions. Figure 5(a) demonstrates one gas inlet, one central outlet, and one annular outlet in our numerical model. A mass flow rate of 22.4 g/s is assigned to the gas inlet boundary. Atmospheric pressure and temperature condition is given to the central outlet. With regard to the third air stream (see Section 2.1), the air could flow from the annulus among drill bit and borehole towards the drill bit or vice versa. Herein, atmospheric pressure and temperature is also applied on the annular outlet. We define the flow direction from the annulus towards drill bit as a positive direction. When air mass flow rate through the annular outlet is positive, air is suctioned from the annulus into drill bit. When the mass flow rate is negative, air escapes from the drill bit. At last, all the walls inside our drill bit model are set to be no-slip and adiabatic surfaces. The wall roughness height is set as 0.1 mm.

Table 2: Mesh independence results.

Number of mesh elements, million	Mass flow rate at inlet, m_0 g/s	Mass flow rate at annular outlet, m_3, g/s	Mass flow rate at central outlet, g/s
0.38	20.5	14.90	35.40
0.46	20.5	15.15	35.65
0.68	20.5	14.11	34.61
0.85	20.5	14.56	35.06
1.09	20.5	14.58	35.08
1.23	20.5	14.49	34.99

3.3. Solution Strategy. Air circulation in our model is mathematically described by compressible steady-state forms of Navier-Stokes (N-S) equations. One of our previous works [6] covered the details of numerical simulations with ANSYS Fluent. In this study, Reynolds stress model is chosen to simulate turbulent air flows inside our drill bit. In addition, we utilized the second-order upwind scheme to discretize the convection diffusion term in N-S equations. Gas in our model is assumed to be an ideal gas whose properties can be easily achieved in Fluent database. The net flux through

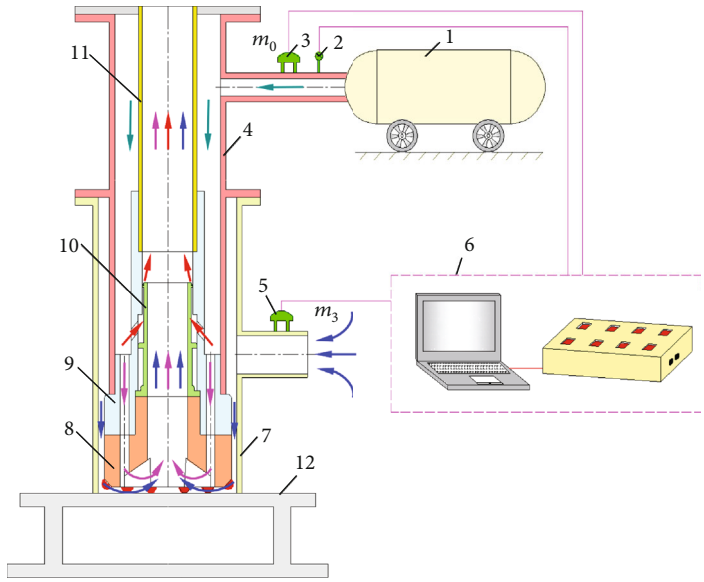

Figure 6: Testing stand of reverse circulation drill bit. 1: air compressor; 2: pressure sensor; 3, 5: air flow meter; 4: outer pipe; 6: data collection system; 7: casing; 8: lower part of the drill bit body; 9: upper part of the drill bit body; 10: swirler; 11: inner pipe; 12: frame.

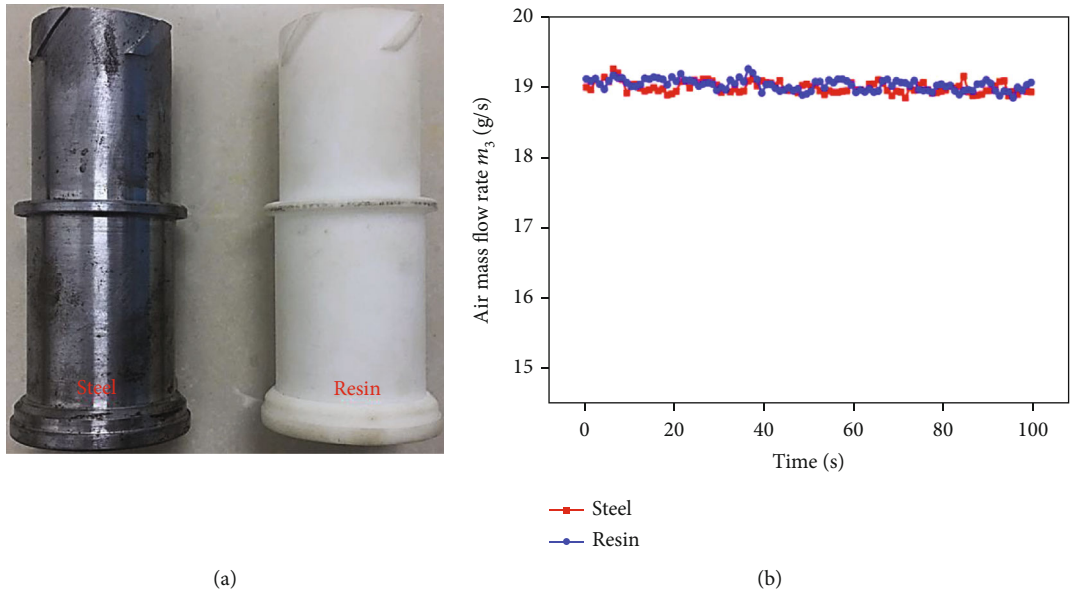

Figure 7: Swirler material test. (a) Swirler; (b) testing results.

the annular outlet is closely monitored to ensure simulation convergence. Moreover, the maximum scale residual of each governing equation in our simulations is set as 10^{-5}.

4. Experimental Measurements

4.1. Testing Stand. Our numerical simulations can be validated by the comparison against experimental results. We have built a testing stand, and all our experiments were completed on the testing stand. Each experiment test would be repeated three times to reduce the likelihood of experimental errors. Figure 6 shows the testing stand of reverse circulation drill bit with a vane swirler inside. As mentioned earlier, drill bit rotation is ignored in this testing stand. A casing works as a simplification of real boreholes. The upper part of the casing is connected with a gas compressor. We add a short section of pipe onto the lower part of the casing. High-pressure air is generated by the gas compressor with a capacity of 1.8 m^3/min and 1.0 MPa. When reverse air circulation starts, ambient air is drawn into the drill bit through this pipe section. A pressure sensor is put at the at the downstream of the gas compressor. One LK-VFF-50 vertex shedding flow meter is located next to the pressure sensor. Another same flow meter is located at the short pipe section. LK-VFF-50 vertex shedding flow meter can measure flow rates in a range of (0.1 g/s, 100 g/s) with 1.5% FS.

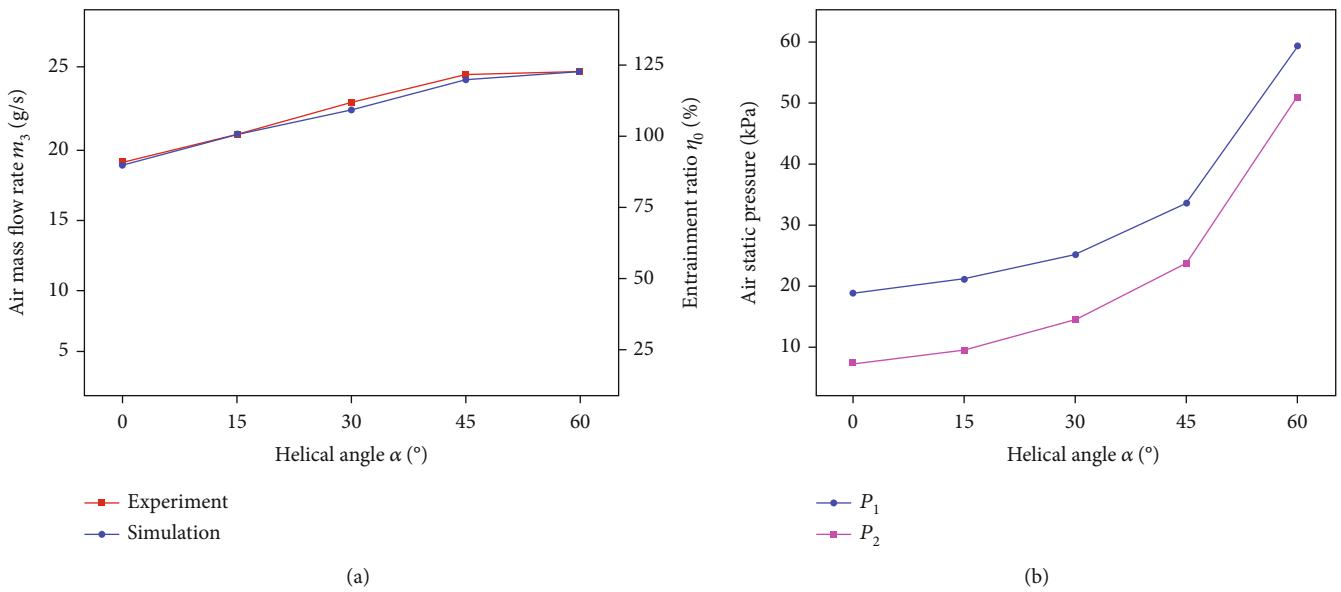

Figure 8: Relationship between helical angle and entrainment performance of drill bit without flushing nozzles: (a) entrainment performance; (b) static pressure.

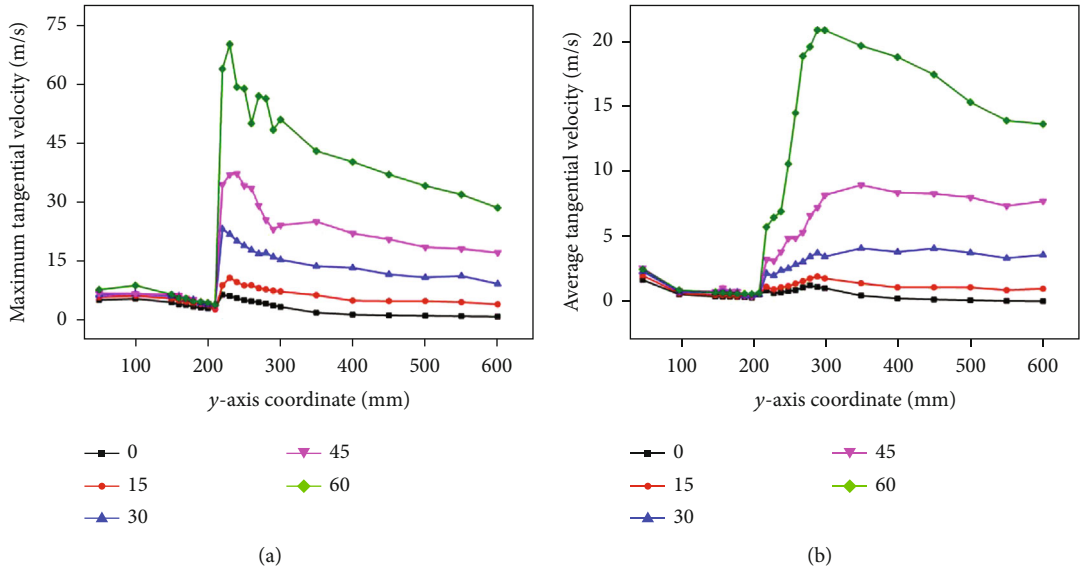

Figure 9: Variations in air velocity at different cross-sections along central passage of drill bit without flushing nozzles: (a) maximum tangential velocity; (b) average tangential velocity.

4.2. Materials. Given the structure and volume of the swirler, it was created by high-resolution laser SLA 3D printing technology using photosensitive resin material. In order to test the impact of the choice of swirler material on the effect of the drill bit, two vane swirlers with the same shape and structural parameters, except materials, were produced as described in Figure 7(a). The number, helical angle, and length of swirler blades were 3, 30°, and 10 mm, respectively. Testing results are given in Figure 7(b). Reverse circulation could effectively form inside the swirling drill bit for both swirlers. At the same operating conditions, the average mass flow rate of air drawn from ambient space for the steel swirler was nearly the same for that made from photosensitive resin. Therefore, using 3D print technology to produce the swirler is considered a reasonable and reliable alternative, since the material seems to have no influence on its performance. The resin swirler test performed in the present study is presented in Figure 7(c).

5. Results and Discussion

5.1. Effect of Blade Helical Angle α. The effect of the blade helical angle α on the reverse circulation of the swirling drill bit without flushing nozzles has been investigated, as shown in Figure 8, while setting the number of spiral blades n and the area ratio λ as 4 and 4, respectively. Both our simulation

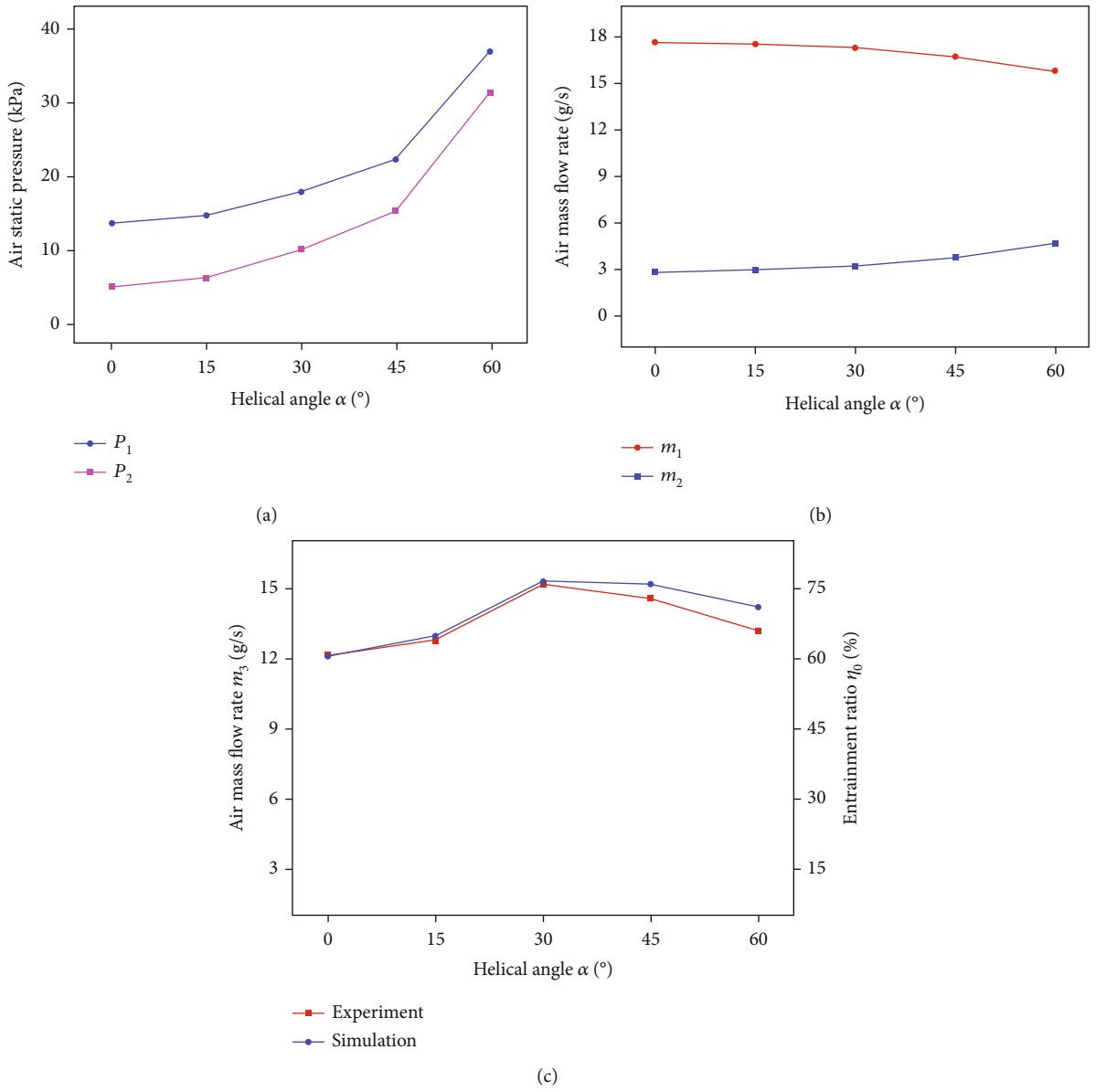

Figure 10: Relationship between helical angle and entrainment performance of drill bit with flushing nozzles: (a) static pressure; (b) air mass flow rate m_1 and m_2; (c) entrainment performance.

and experimental results indicate that the air mass flow rate m_3, suctioned into the drill bit from the annulus between the drill bit and the borehole wall, increases almost linearly with increased blade helical angle. Its value improves from 18.49 g/s to 25.22 g/s when the helical angle is increased from 0° to 60° in the experiment, while it rises from 18.66 g/s to 25.27 g/s in the simulation, indicating that the simulations agree very well with experimental results. The maximum divergence between simulation and experimental results is 2.32%. Moreover, as clearly seen in Figure 8(a), the entrainment ratio rises with increased helical angle, since the mass flow rate of air suctioned into the drill bit is correspondingly improved. When the helical angle is 60°, this ratio is determined as 123.33%.

It should be noted that the blade helical angle of the swirler has an important influence on the pressure of air flowing through the drill bit, as described in Figure 8(b). A larger helical angle results in more air pressure resistance in a drill bit; the air pressure shows a marked increase, especially when the helical angle is larger than 30° and rises further.

Figure 9 displays the variations of tangential air velocity along the drill bit's central passage under different casing cross-section areas. As can be seen in Figure 9, the gas ejected from the vane swirler has high tangential velocities. It reaches its maximum value near the outlet of the spiral slot, then decreases gradually along the central passage of the drill bit. The larger the helical angle, the higher the maximum tangential velocity value, and the faster the decay of the tangential component of the air velocity, as indicated in Figure 9(a). Entrainment effect of swirling flows would draw ambient air into drill bit. Then, this air flow is mixed

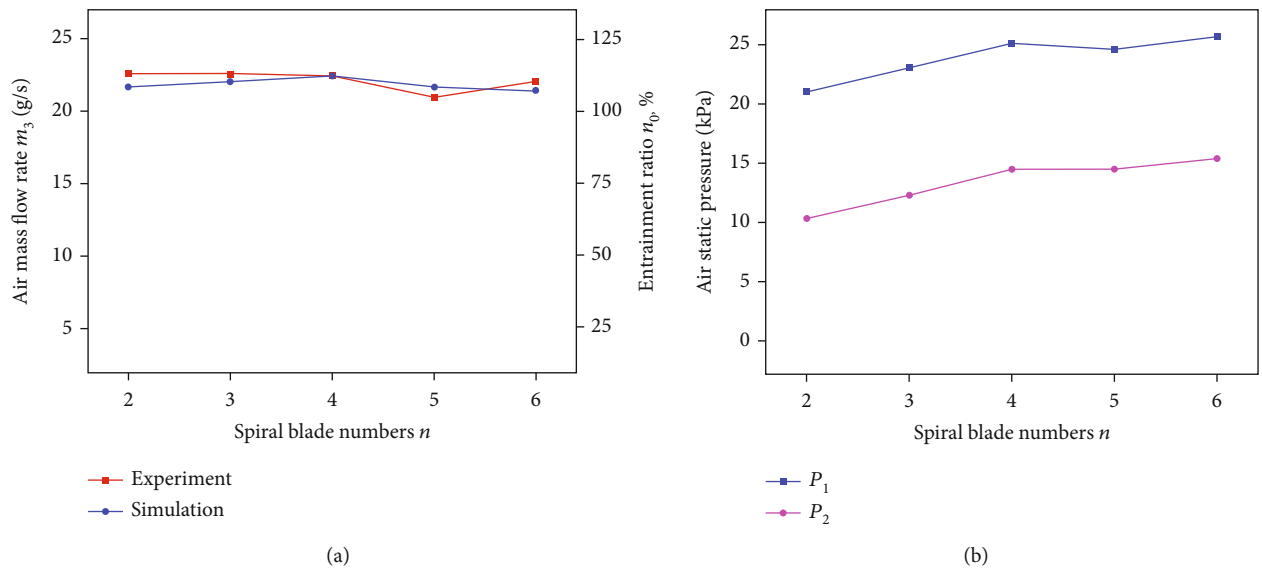

Figure 11: Relationship between number of spiral blades and entrainment performance of drill bit without flushing nozzles: (a) entrainment performance; (b) static pressure.

with the swirling flow at the spiral slots. The mixture continues to flow forward until being exhausted from the drill bit. In this process, the suctioned air flow is accelerated, while the primary swirling flow is decelerated, which is the main reason why the average tangential velocity still grows at some distance after passing through the spiral slots, as shown in Figure 9(b).

If all other parameters are kept unchanged, and the flushing nozzles of the drill bit are opened for testing, results are obtained as described in Figure 10. The variation trend of the static air pressure resistance for the drill bit with opened flushing nozzles is similar to that without flushing nozzles under the same helical angle conditions, while its value is smaller. When the helical angle of the spiral blade is increased from 0° to 60°, the static pressure nearby the inlet of the swirler rises from 5.09 kPa to 31.47 kPa, which is an over sixfold increase. Under the conditions of larger helical angle, more air will be exhausted from the flushing nozzles, since the flow resistance of the swirler increases (as shown in Figure 10(b)). When the helical angle is increased from 0° to 60°, the mass flow rate of air through the flushing nozzles rises from 2.82 g/s to 4.69 g/s and correspondingly reduces from 17.68 g/s to 15.81 g/s when ejected from the swirler. This may be the main reason why the entrainment performance of the drill bit begins to weaken when the helical angle of the spiral blade exceeds 30° (as indicated in Figure 10(c)).

It is worth noting that the entrainment performance of the drill bit with flushing nozzles is considerably worse than that of the drill bit without flushing nozzles under the same conditions. For example, the entrainment ratio is 109.53% for the drill bit without flushing nozzles under the case of helical angle 30°, while it is reduced to 75.83% if the flushing nozzles are opened. When the helical angle is increased to 60°, the ratio is approximately 123.01% for the drill bit without flushing nozzles, while it is reduced by about half (65.94%) for opened flushing nozzles.

5.2. Effect of n Number of Spiral Blades. With a helical angle of the spiral blade of $\alpha = 30°$ and an area ratio of $\lambda = 4$, the effect of n number of spiral blades on the reverse circulation of the swirling drill bit without flushing nozzles was investigated (as shown in Figure 11). It is clearly seen that the number of spiral blades has little influence on the entrainment performance of the drill bit. When the number of blades is increased from 2 to 6 in experiments, the entrainment ratio varies between 107.71% and 110.38%, while the static pressure nearby the inlet of the swirler P_2 increases gradually from 10.34 kPa to 15.43 kPa.

If the flushing nozzles of the drill bit are opened and all other parameters are kept unchanged, the influence of number of blades on swirler entrainment performance is obtained as given in Figure 12. The air static pressure $P1$ increases slightly with an increased number of spiral blades, while the air mass flow rate $m1$ and $m2$ remain nearly unchanged. Accordingly, the reverse circulation performance of the drill bit is also less affected (as shown in Figure 12(c)). In addition, the flushing nozzles have an important effect on the entrainment performance of the drill bit. It takes a value of 110.02%, for example, when the n number of spiral blades is 3 for the drill bit without flushing nozzles, while it is reduced to 76.55% when the flushing nozzles are opened.

5.3. Effect of Area Ratio λ. The area ratio λ, defined as the ratio of total outlet area of the spiral slots to that of flushing nozzles as mentioned above, can be altered by varying the central angle of the spiral blade θ. For a drill bit without flushing nozzles, the outlet area of the swirler is the same as that of the drill bit with flushing nozzles under the same conditions. Therefore, the area ratio λ is also used to describe the outlet area of the drill bit without flushing nozzles.

Given the number of spiral blades as $n = 3$, and the helical angle as $\alpha = 30°$, the effect of area ratio on the

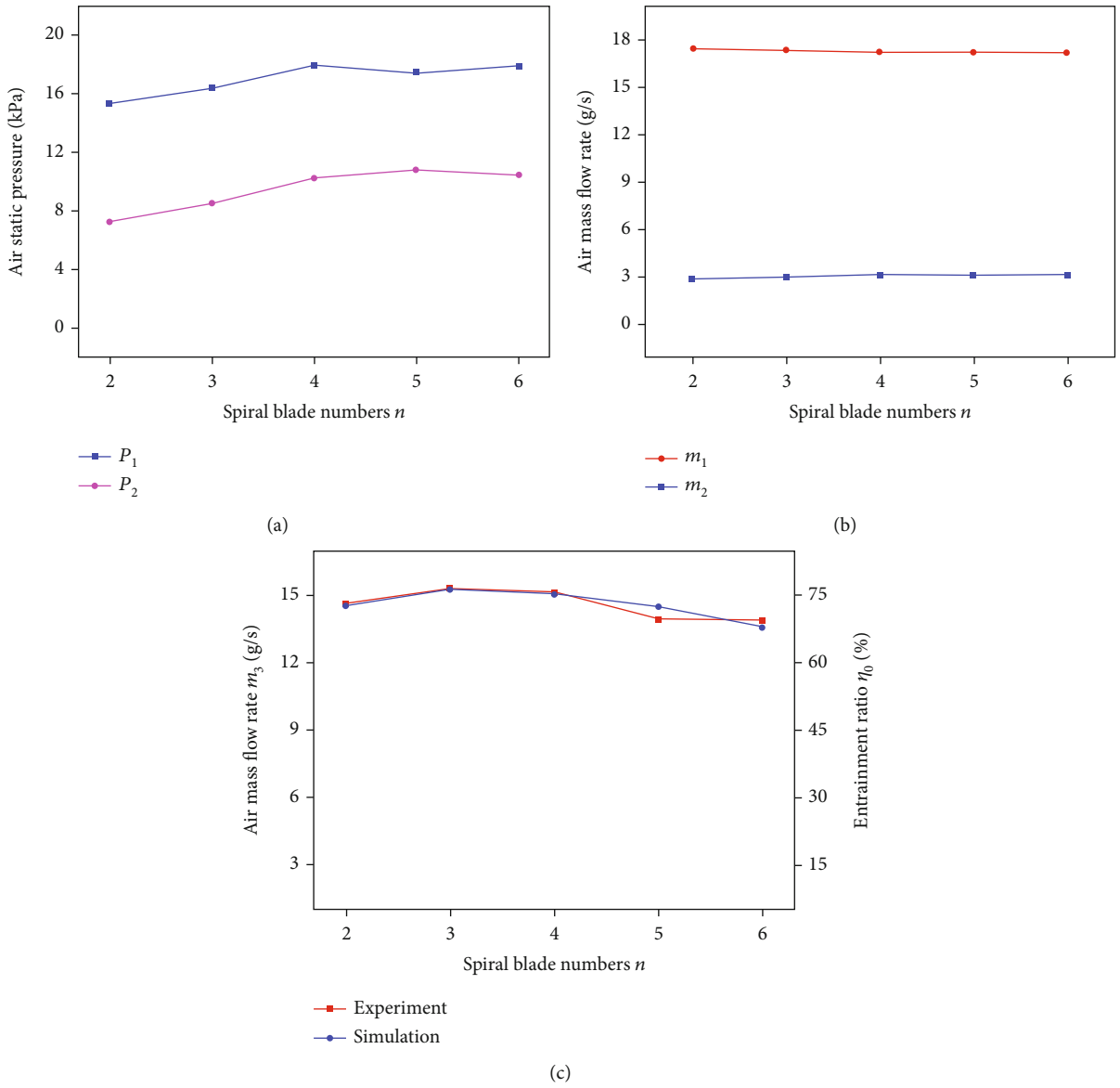

Figure 12: Relationship between number of spiral blades and entrainment performance of drill bit with flushing nozzles: (a) static pressure; (b) air mass flow rate m_1 and m_2; (c) entrainment performance.

entrainment performance of the swirling drill bit without flushing nozzles was investigated (as presented in Figure 13). The area ratio is clearly an important parameter influencing the entrainment performance of the swirling drill bit. The maximum value of the entrainment ratio η_0 occurs at an area ratio of 2, which is equivalent to 144.89% in the experiment. This is because the pressure resistance of air flowing through the swirler is higher if the area ratio is too small, resulting in a significant energy loss. Meanwhile, the velocity of air ejected from the swirler will be reduced if the area ratio is too large, which weakens the suctioning effect. With the area ratio increased from 1 to 4, the static pressure nearby the swirler inlet decreases rapidly from 221.86 kPa to 12.26 kPa (as illustrated in Figure 13(b)).

The relationship between the area ratio and entrainment performance of the drill bit with flushing nozzles is demonstrated in Figure 14. Like that of the drill bit without flushing nozzles, the static pressure of air flowing through the swirler decreases quickly with increased area ratio λ, which leads to the reduction of air mass flow rate m_2 at the same time. When the value of λ is increased from 1 to 4, the static pressure P_2 declines from 102.97 to 8.54 kPa, while the value m_2 is reduced from 8.49 to 3.21 g/s. Accordingly, the mass flow rate of air ejected from the swirler improves from 12.01 to 17.29 g/s, which is beneficial for improved entrainment performance of the drill bit. It should be noted, however, that the air velocity will be reduced when the area ratio λ is increased to more than 3 despite the elevated mass flow rate through the swirler (as illustrated in Figure 14(c)). When the value of λ is increased from 3 to 4, the maximum air velocity from the swirler declines from 133.27 to 90.92 m/s. This could be the main reason why the entrainment ratio of the

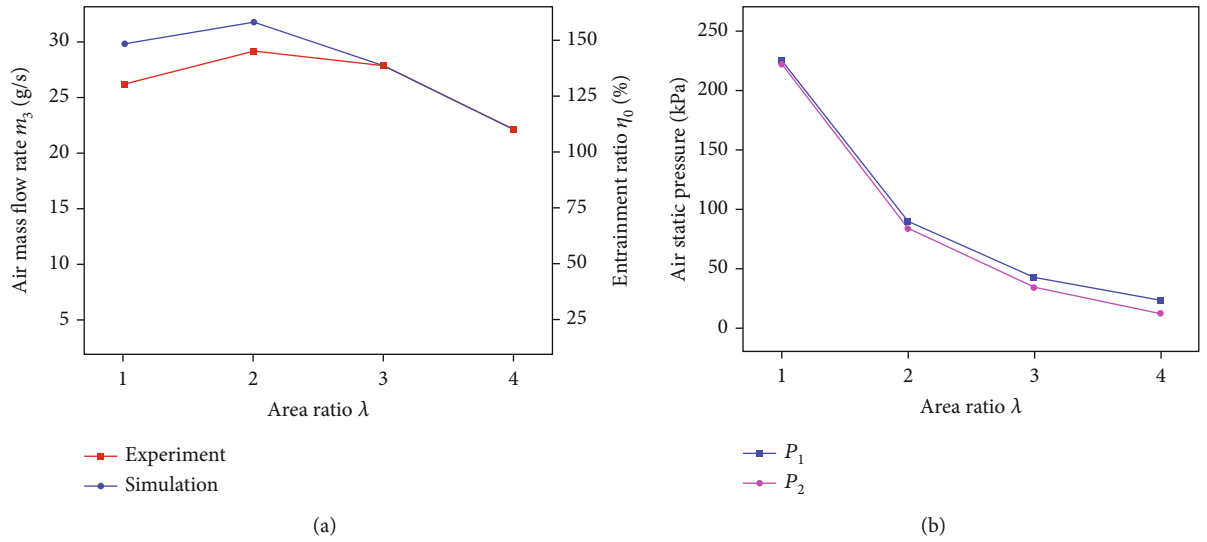

FIGURE 13: Relationship between area ratio and entrainment performance of drill bit without flushing nozzles: (a) entrainment performance; (b) static pressure.

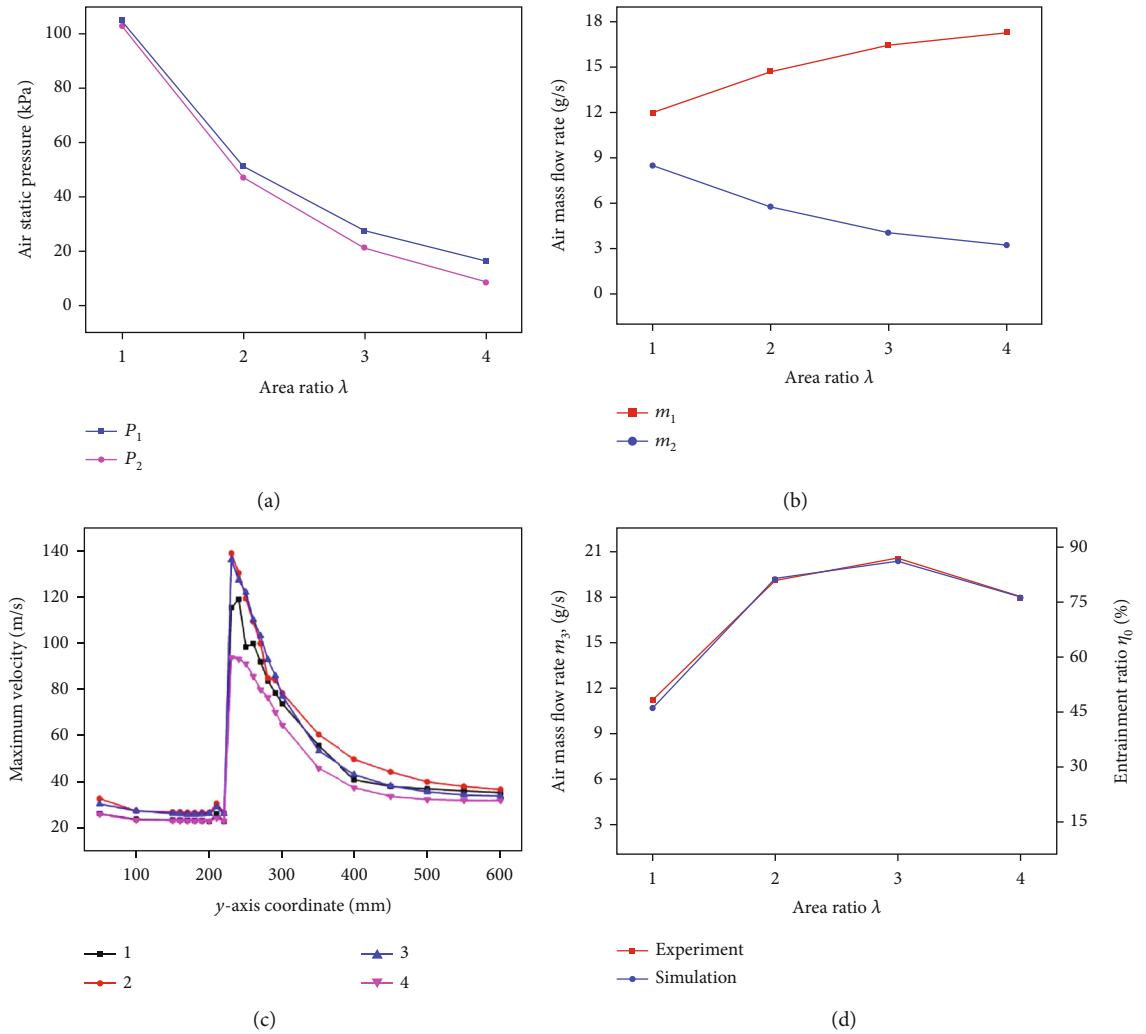

FIGURE 14: Relationship between area ratio and entrainment performance of drill bit with flushing nozzles: (a) static pressure; (b) air mass flow rate m_1 and m_2; (c) maximum velocity; (d) entrainment performance.

drill bit shows a rising trend from 48.11 to 86.88% with λ increased from 1 to 3 and decreases to 76.55% when λ is further increased to 4 (as shown in Figure 14(d)).

6. Conclusions

(1) The reverse circulation performance of a novel swirling drill bit design was evaluated by CFD simulation and experimental investigations. The numerical calculation results obtained were in reasonable agreement with the experimental data. The maximum error between simulation and experimental results was only 13.68%, which occurred for the case of drill bit without flushing nozzles

(2) It was observed that several parameters, including the helical angle, the number of spiral blades, and the outlet area of the swirler, may affect the reverse circulation performance of the swirling drill bit, regardless of whether the drill bit was designed with flushing nozzles or not. Among these parameters, the effect of the area ratio was the most obvious one, while the number of spiral blades had the smallest influence. For the drill bit without flushing nozzles, the optimal parameters were a helical angle of 60°, 4 spiral blades, and an area ratio of 2, while those for the drill bit designed with flushing nozzles were 30°, 3, and 3, respectively

(3) Flushing nozzles have a significant impact on the reverse circulation performance of the swirling drill bit. Compared with the drill bit designed with flushing nozzles, the entrainment ratio of the drill bit without one can be improved by more than twice under the same conditions. Therefore, the method of sealing flushing nozzles can be employed to improve the reverse circulation effect during the drilling process

Data Availability

Some or all data, models, or code generated or used during the study are available from the corresponding author by request (jlucpl@jlu.edu.cn).

Conflicts of Interest

The authors declare no competing interests.

Acknowledgments

This paper presents results of the research done under support of the Scientific Research Project of Zhejiang Provincial Department of Housing and Urban-Rural Development (project no. 2018K105) and the Scientific Research Project of Zhejiang Engineering Survey and Design Institute Group Co. Ltd. (project no. 2019-008).

References

[1] G. C. Yao, J. Zhao, X. B. Shen, H. E. Yang, and D. S. Wen, "Effects of rheological properties on heat transfer enhancements by elastic instability in von-Karman swirling flow," *International Journal of Heat and Mass Transfer*, vol. 152, p. 119535, 2020.

[2] A. A. Verbeek, T. W. F. M. Bouten, G. G. M. Stoffels, B. J. Geurts, and T. H. van der Meer, "Fractal turbulence enhancing low-swirl combustion," *Combustion, and flame*, vol. 162, no. 1, pp. 129–143, 2015.

[3] L. Dong and A. Rinoshika, "Comparison between rotation swirler and non-rotation swirler in a horizontal swirling flow pneumatic conveying," *Powder Technology*, vol. 346, pp. 396–402, 2019.

[4] Z. Tianxing, L. Khezzar, M. AlShehhi, Y. Xia, and Y. Hardalupas, "Experimental investigation of air-water turbulent swirling flow of relevance to phase separation equipment," *International Journal of Multiphase Flow*, vol. 121, pp. 103–110, 2019.

[5] P. Balakrishnan and K. Srinivasan, "Jet noise reduction using co-axial swirl flow with curved vanes," *Applied Acoustics*, vol. 126, pp. 149–161, 2017.

[6] P. L. Cao, M. M. Liu, Z. Chen, B. Y. Chen, and Q. Zhao, "Theory calculation and testing of air injection parameters in ice core drilling with air reverse circulation," *Polar Science*, vol. 17, pp. 23–32, 2018.

[7] B. M. Chen, K. Ho, Y. S. Abakr, and A. Chan, "Fluid dynamics and heat transfer investigations of swirling decaying flow in an annular pipe part 1: review, problem description, verification and validation," *International Journal of Heat and Mass Transfer*, vol. 97, pp. 1029–1043, 2016.

[8] M. G. Yehia, A. A. A. Attia, O. E. Abdelatif, and E. E. Khalil, "Heat transfer and friction characteristics of shell and tube heat exchanger with multi inserted swirl vanes," *Applied Thermal Engineering*, vol. 102, pp. 1481–1491, 2016.

[9] C. Wen, A. Q. Li, J. H. Walther, and Y. Yang, "Effect of swirling device on flow behavior in a supersonic separator for natural gas dehydration," *Separation and Purification Technology*, vol. 168, pp. 68–73, 2016.

[10] H. Funahashi, K. Hayashi, S. Hosokawa, and A. Tomiyama, "Study on two-phase swirling flows in a gas-liquid separator with three pick- off rings," *Nuclear Engineering and Design*, vol. 308, pp. 205–213, 2016.

[11] W. Liu and B. F. Bai, "Swirl decay in the gas-liquid two-phase swirling flow inside a circular straight pipe," *Experimental Thermal and Fluid Science*, vol. 68, pp. 187–195, 2015.

[12] M. F. Strauss, S. L. Story, and N. E. Mehlhorn, "Applications of dual-wall reverse-circulation drilling in ground water exploration and monitoring," *Groundwater Monitoring & Remediation*, vol. 9, no. 2, pp. 63–71, 1989.

[13] J. F. He, B. X. Sun, Y. P. Liang, and Y. J. Luo, "Research on suction capacity and dust suppression performance of a reverse circulation air hammer in tunnel drilling," *Tunnelling and Underground Space Technology*, vol. 71, pp. 391–402, 2018.

[14] P. L. Cao, Q. Zhao, Z. Chen, H. Y. Cao, and B. Y. Chen, "Orthogonal experimental research on the structural parameters of a novel drill bit used for ice core drilling with air reverse circulation," *Journal of Glaciology*, vol. 65, no. 254, pp. 1011–1022, 2019.

[15] Q. L. Yin, J. M. Peng, K. Bo, J. F. He, Y. L. Kui, and X. Gan, "Study on dust control performance of a hammer drill bit,"

International Journal of Mining, Reclamation and Environment, vol. 27, no. 6, pp. 393–406, 2013.

[16] S. B. Thomas, *Fluid Flow Control Means for a Reverse Circulation Down Hole Hammer*, World Intellectual Property Organization, Canning Vale, Australia, 2007, WO2007/062490.

[17] J. C. Green, "Rock drilling equipment.," 2008, US Patent 7467674B2, 2008.

[18] Y. J. Luo, J. M. Peng, L. J. Li et al., "Development of a specially designed drill bit for down-the-hole air hammer to reduce dust production in the drilling process," *Journal of Cleaner Production*, vol. 112, pp. 1040–1048, 2016.

[19] B. Qi, P. L. Cao, H. Yang et al., "Experimental and numerical study on air flow behavior for a novel retractable reverse circulation drill bit of casing-while-drilling (CwD)," *Geofluids*, vol. 2021, 12 pages, 2021.

[20] D. Y. Wu, K. Yin, Q. L. Yin et al., "Reverse circulation drilling method based on a supersonic nozzle for dust control," *Applied Sciences*, vol. 7, no. 1, pp. 5–15, 2017.

[21] P. L. Cao, Y. W. Chen, M. M. Liu, B. Y. Chen, and J. S. Wang, "Analytical and experimental study of a reverse circulation drill bit with an annular slit," *Advances in Mechanical Engineering*, vol. 8, no. 9, 2016.